Simulation of vapor-liquid coexistence in finite volumes: A method to compute the surface free energy of droplets

Manuel Schrader, Peter Virnau,* and Kurt Binder
Institute of Physics, Johannes-Gutenberg-Universität Mainz, Staudinger Weg 7, D-55099 Mainz, Germany
(Received 20 March 2009; published 9 June 2009)

When a fluid at a constant density ρ in between the densities of coexisting vapor (ρ_v) and liquid (ρ_ℓ) at temperatures below criticality is studied in a (cubic) box of finite linear dimension L, phase separation occurs in this finite volume, provided L is large enough. For a range of densities, one can observe a liquid droplet (at density ρ_ℓ' slightly exceeding ρ_ℓ) coexisting in stable thermal equilibrium with surrounding vapor (with density $\rho_v' > \rho_v$, so in the thermodynamic limit such a vapor would be supersaturated). We show, via Monte Carlo simulations of a Lennard-Jones model of a fluid and based on a phenomenological thermodynamic analysis, that via recording the chemical potential μ as function of ρ, one can obtain precise estimates of the droplet surface free energy for a wide range of droplet radii. We also show that the deviations of this surface free energy from the prediction based on the "capillarity approximation" of classical nucleation theory (i.e., using the interfacial free energy of a flat liquid-vapor interface for the surface free energy of a droplet irrespective of its radius) are rather small. We also study carefully the limitation of the present method due to the "droplet evaporation/condensation transition" occurring for small volumes and demonstrate that very good equilibrium is achieved in our study, by showing that the radial profile of the local chemical potential from the droplet center to the outside is perfectly flat.

DOI: 10.1103/PhysRevE.79.061104 PACS number(s): 64.60.an, 64.60.qe, 05.70.Np

I. INTRODUCTION AND OVERVIEW

The concept of nucleation as a mechanism of a phase change in a thermodynamic system that can exist in several phases is a classical concept [1–5] but nevertheless not well understood until today (see, e.g., [6–16] for a small collection of relevant literature). The archetypical problem is the spontaneous formation of a liquid droplet from a slightly supersaturated vapor due to statistical fluctuations ("homogeneous nucleation"). According to classical nucleation theory [1–11,14] one constructs the work of formation of such a droplet. The free-energy barrier ΔF^* that needs to be overcome in a nucleation event can be expressed in terms of a competition of bulk and surface free energies of a droplet. Assuming a spherical droplet of radius R, and assuming further that the surface free energy of the droplet is identical to the interfacial free energy (per unit area) $\gamma_{v\ell}$ of a macroscopic flat interface between bulk coexisting vapor and liquid phases, one arrives at a free energy $\Delta F(R)$,

$$\Delta F(R) = -\frac{4\pi R^3}{3}\Delta p + 4\pi R^2 \gamma_{v\ell}. \tag{1}$$

At constant temperature and chemical potential (note that in equilibrium the droplet and the surrounding vapor can freely exchange both energy and particles) the bulk free-energy difference per unit volume between the liquid drop and the surrounding vapor is just the pressure difference Δp, of course. For small R the positive second term on the right-hand side of Eq. (1) dominates, and so a barrier ΔF^* results. The corresponding maximum of $\Delta F(R)$ occurs at the critical radius R^*. The derivation $d\Delta F(R)/dR|_{R=R^*}=0$ yields $R^* = 2\gamma_{v\ell}/\Delta p$.

Physically relevant barriers (which lead to nucleation rates on physically observable time scales, e.g., of the order of 1 to 10^6 nucleation events per cubic centimeter and second) are somewhere in the range from $20k_BT$ to $100k_BT$ (depending on the considered system and the assumptions needed to draw conclusions on the nucleation rate from the nucleation barrier [6–11]). One easily recognizes a serious problem: apart from the immediate vicinity of the critical point where $\gamma_{v\ell}$ vanishes [10,17] the resulting values of R^* are of the order of a few molecular diameters. Hence, there is no reason to expect that a macroscopic description of such nanodroplets as suggested in Eq. (1) should be accurate. In fact, since ΔF^* scales like the third power of $\gamma_{v\ell}$,

$$\Delta F^* = \frac{16\pi}{3}\frac{\gamma_{v\ell}^3}{\Delta p^2}, \tag{2}$$

and the nucleation rate J depends on ΔF^* via an Arrhenius relation,

$$J = \nu^* \exp\left(\frac{-\Delta F^*}{k_BT}\right), \tag{3}$$

relative errors of 10% for $\gamma_{v\ell}$ lead to relative errors of 30% in ΔF^*. Therefore the error in J may easily span several orders of magnitude. In Eq. (3), T is the absolute temperature, k_B is Boltzmann's constant, and the prefactor ν^* may contain various corrections resulting from a more detailed consideration of the kinetics of the nucleation process ("Zeldovitch factor" [3], description of nucleation as a flow over a saddle point in a multidimensional phase space [7,10] rather than describing droplets by a single degree of freedom, R, etc. [6–16]).

*virnau@uni-mainz.de

A first step to go beyond the capillarity approximation for small droplets was proposed by Tolman [18], who introduced the phenomenological Tolman length δ to describe the curvature dependence of the surface tension $\gamma(R)$ of small droplets as follows:

$$\gamma(R) = \frac{\gamma_{v\ell}}{(1+2\delta/R)}. \quad (4)$$

It is difficult to give δ a more precise meaning in the context of statistical mechanics and the dependence of δ on temperature is still under discussion [19–22]. Using Eq. (4) in Eq. (1) for large R leads to a correction linear to R to Eq. (1). Of course, for small R many other corrections may come into play, e.g., logarithmic terms ($\propto \ln R$) as proposed in Fisher's droplet model [23], which is believed to be relevant near the critical point [10,11]. Another important fact is that the vapor-liquid interface on the molecular scale is diffuse rather than sharp [17], and hence the separation of ΔF into bulk and interfacial terms is clearly problematic [13,24]. Thus, the theoretical understanding of homogenous nucleation is still unsatisfactory.

Of course, there have been many attempts to explore homogenous nucleation via experiments (for some recent examples see [25–27]). However, experimental studies of homogeneous nucleation of liquid droplets in supersaturated vapors are very difficult for several reasons: (i) The small size of critical droplets and their extremely small density make a direct observation of critical droplets impossible. Only when they have grown to a size much larger than the critical size can droplets be detected by light scattering methods [25–27]. (ii) One has to avoid very carefully any heterogeneous nucleation at the wall of the container, at dust particles, or ions, etc. Heterogeneous nucleation agents may reduce ΔF^* dramatically, and hence even a tiny concentration of such agents may falsify the measurement. Of course, if an experimentally observed deviation from the classical nucleation theory implies a too high free-energy barrier, such a discrepancy cannot be attributed to the effect of heterogeneous mechanisms, which could only reduce the barrier rather than enhancing it. Experiments on nucleation in argon [26], a particularly simple fluid composed of neutral pointlike atoms interacting with a potential similar to simple Lennard-Jones forces, have revealed unexplained discrepancies in the nucleation rate of up to a factor 10^{26} between the prediction of classical nucleation theory and measurement.

Computer simulations, on the other hand, do not suffer from the problem of heterogeneous nucleation at all. Walls are avoided by using periodic boundary conditions and no dust particles or any other kinds of impurities occur. In addition, observations on scales down to the nanoscale or even the scale of single atoms are readily possible, because in simulations one has full information on the coordinates of all the atoms. Nevertheless, the study of nucleation events by simulation is very difficult, since for $\Delta F^* \gg k_B T$, nucleation events are very rare: one would have to simulate huge systems over very long time scales (note that for molecular-dynamics methods [28] the typical time scales range from picoseconds to at most microseconds). Thus simulation studies of nucleation kinetics have often addressed very simplified models, such as the lattice gas (Ising) model, and very high supersaturation, where the nucleation barrier ΔF^* is down to a few $k_B T$, e.g., [10,29–33]. Only by implementing the novel technique of transition path sampling [34] can this limitation be overcome and trajectories can be sampled that correspond to nucleation events over barriers in the physically interesting range [35]. Even though for the Ising model this approach is very promising, it is still in an exploratory stage [36].

As an alternative, rather early the idea was proposed to use simulation to directly study a critical droplet which is stabilized by confining the droplet in a small box [9,37,38]. A drawback of these early studies was that all particles in the box were counted as belonging to the droplet, while in reality the system contains a droplet in equilibrium with supersaturated vapor [39]. It was suggested to use the Stillinger neighborhood criterion [40] to define which particles belong to the droplet. Such an approach was later used by ten Wolde and Frenkel [41,42], who used biased Monte Carlo algorithms ("umbrella sampling" [43,44]) to stabilize large droplets in their simulation. However, possible corrections due to finite-size effects have not been studied in this approach. Homogeneous and heterogeneous nucleation of single crystal nuclei were also considered in subsequent studies [45–47] as well as more complex systems such as crystallization of hard-rod liquids [48] and anisotropic colloids [49].

A systematic approach to study the equilibrium between a droplet and surrounding supersaturated vapor in a finite volume was attempted in [50] in terms of a phenomenological theory and Monte Carlo simulations for the Ising lattice gas model (see also [51]). It was pointed out that the equilibrium between the droplet and the surrounding vapor is only stable if the total density ρ exceeds a density ρ_t which depends on the box linear dimensions L such that

$$\rho_t - \rho_v \propto L^{-3/4}. \quad (5)$$

In the region $\rho_v < \rho < \rho_t$ the homogeneous vapor (which would be supersaturated in the thermodynamic limit) is the thermodynamically stable phase. The so-called "droplet evaporation/condensation transition" at $\rho = \rho_t$ has received considerable attention recently [52–60], but is not in the main focus of the present work. Rather the goal of the present work is the use of the equilibrium properties of the vapor coexisting with the droplet to obtain information on the surface free energy of the droplet, over a wide range of R. While a related analysis was attempted in [51] for the lattice gas model near the critical point, the analysis of [51] was inconclusive due to insufficient statistics. The system sizes available in that study were also too small, and also the value used for $\gamma_{v\ell}$ [61] was somewhat inaccurate. First results of the free energy of droplets as a function of radius using a simplified model were already published in [62].

Figure 1 illustrates the main idea of our analysis: for a fluid of point particles interacting with Lennard-Jones forces at temperature $T = 0.68 T_c$ in a cubic box of size $L = 15.8\sigma$ (the Lennard-Jones parameter σ sets the length scale in our problem) the chemical potential difference $\hat{\mu} = \mu(N) - \mu$ with $\mu = \mu_{coex}$ is plotted versus density. One can see a curve with a maximum, and a minimum, and several rounded kinks. All

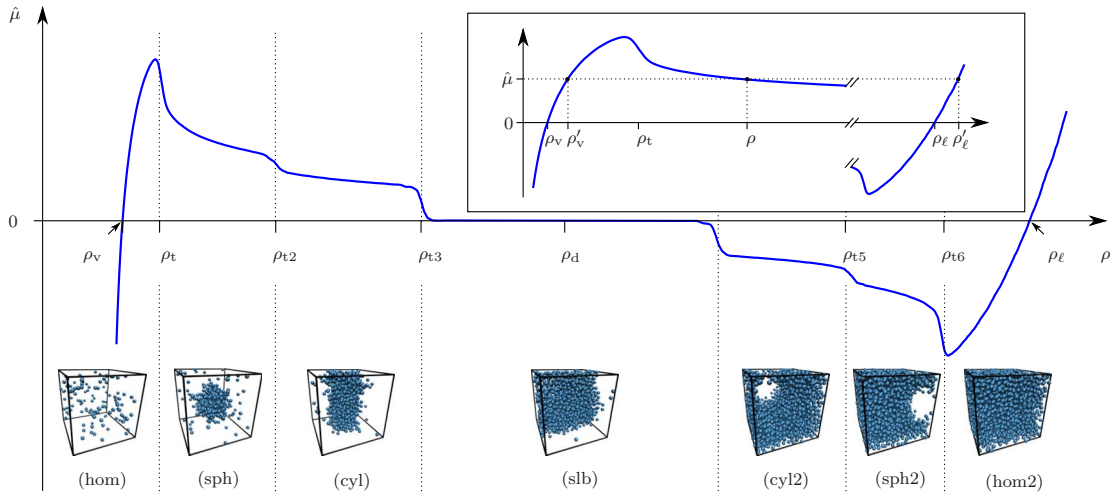

FIG. 1. (Color online) Chemical potential difference $\hat{\mu}=\mu(N)-\mu_{\text{coex}}$ plotted vs density ρ for a cubic $L\times L\times L$ box of size $L=15.8\sigma$ (σ is the Lennard-Jones diameter) at $T=0.68T_c$. The states at $\hat{\mu}=0$ with density ρ_v (vapor) and ρ_ℓ (liquid) approximate very accurately the homogeneous phases that can coexist in the thermodynamic limit. In the finite box, the homogeneous vapor (indicated by the snapshot picture denoted as "hom") also exists for densities exceeding ρ_v, up to about the density ρ_t (dotted vertical line) where the droplet evaporation/condensation transition occurs. For densities from about ρ_t to about ρ_{t2} the system is in an inhomogeneous state. A spherical (sph) droplet coexists with surrounding supersaturated vapor. At ρ_{t2} the shape of the liquid droplet changes from spherical to cylindrical (cyl), which is the stable two-phase configuration for $\rho_{t2}<\rho<\rho_{t3}$, while in the central region around $\rho_d=(\rho_\ell+\rho_v)/2$ a slablike two-phase configuration (slb) is stable ($\rho_{t3}<\rho<\rho_{t4}$). At ρ_{t4} the character of two-phase coexistence in the box changes again. The vapor changes from a slablike region to a cylindrical domain (cyl2), while for $\rho_{t5}<\rho<\rho_{t6}$ one has a coexistence of a spherical bubble (sph2) with surrounding liquid. Inset: this graph illustrates that for $\hat{\mu}>0$ there exists a regime of $\hat{\mu}$ where three phases correspond to the same value of $\hat{\mu}$ and hence can coexist with each other—a homogeneous vapor at density $\rho'_v>\rho_v$, a homogeneous liquid droplet coexists with surrounding vapor, at average density ρ (in the regime $\rho_t<\rho<\rho_{t2}$) in the simulation box, and a homogeneous liquid at density ρ'_ℓ. Note that the occurrence of all these phases was already discussed in [56,57].

these features indicate (rounded) transitions between different states of the system, as illustrated by the small snapshot pictures in the lower part of the figure. The region of interest is the first descending part of the $\hat{\mu}$ vs ρ curve. Here, a spherical droplet coexists with surrounding vapor. The key observation is that at the chemical potential difference $\hat{\mu}$, there exist two pure phases at the ascending branches of the $\hat{\mu}$ vs ρ curve: a pure vapor on the left branch and a pure liquid at the right branch. Accepting the principle that states that have the same chemical potential can coexist with each other, we conclude that the vapor in the mixed-phase state at the descending branch of the $\hat{\mu}$ vs ρ curve is identical in its properties (in particular, its density) with the pure vapor. The density inside of the liquid droplets is the same as the density of the pure fluid at the same chemical potential. As will be shown in Sec. III, the knowledge of the densities ρ'_v, ρ, and ρ'_ℓ taken from Fig. 1 (inset) allows to infer the droplet radius R from a purely thermodynamic construction. An alternative estimate in terms of the Stillinger criterion [40] yields identical results (Sec. V). Thermodynamic integration of the $\hat{\mu}$ vs ρ curve yields the free energy of the mixed phase state, from which the droplet surface free energy can be extracted (Sec. III). Of course, the range of $\hat{\mu}$ and of R that can be studied from one such curve as shown in Fig. 1 is limited; but if we vary L a wide range of R is accessible. As an example, Fig. 2 shows a snapshot for $L=33.7\sigma$ with a droplet containing $N=3427$ atoms.

The outline of our paper is as follows: in Sec. II we briefly review our simulation methodology, while Sec. III describes the theoretical basis of our analysis in more detail. Section IV gives more details on the droplet evaporation/condensation transition, while Sec. V describes the main results of our study, and discusses the consequences on the behavior of the nucleation barrier ΔF^*. Section VI concludes our paper and gives an outlook on future work.

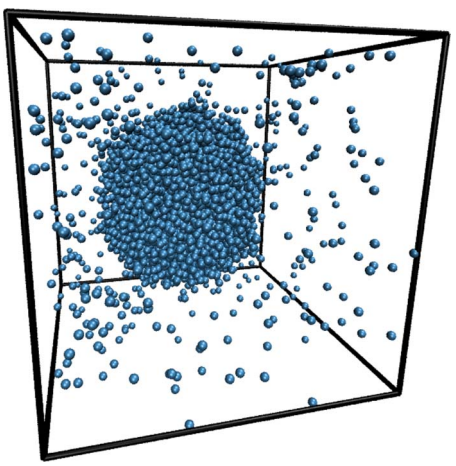

FIG. 2. (Color online) Typical snapshot picture of a spherical droplet in a box of linear dimension $L=33.7\sigma$ at average density $\rho=0.1\sigma^{-3}$ (total particle number $N=3827$ and $N=3427$ particles in the droplet).

II. MODEL AND SIMULATION TECHNOLOGY

For simplicity, we consider point particles which interact with Lennard-Jones forces. The potential is truncated and shifted to zero (since then the code runs significantly faster than for the untruncated potential),

$$u(r) \equiv \begin{cases} 4\epsilon\left\{\left(\frac{\sigma}{r}\right)^{12} - \left(\frac{\sigma}{r}\right)^{6}\right\} + C, & r \le r_c \\ 0, & r > r_c, \end{cases} \tag{6}$$

where ϵ describes the depth of the potential well and σ describes the range of the potential. The constant $C=\frac{127}{16\,384}$ is chosen such that $u(r)$ is continuous at $r=r_c$. We choose a rather small value for r_c, namely, $r_c=2\cdot 2^{1/6}\sigma$ (=twice the distance of the minimum). For this choice the critical temperature is known to be $T_c \approx 0.999\epsilon/k_B$ [63]. Although this value is about 30% lower than the corresponding value $T_c \approx \epsilon/k_B$ [64] of the untruncated potential (only the latter can be taken as an almost realistic model of the actual interaction between argon atoms, as used in the experiments [26,27]), it has been shown that the properly rescaled phase diagram of the truncated model in the $T-\rho$ plane almost coincides with the phase diagram of the untruncated model [65]. Thus we think that no essential physics with respect to the vapor-liquid transition has been lost by this truncation.

As usual, we apply cubic $L\times L\times L$ simulation boxes with periodic boundary conditions throughout, with $11.3\sigma \le L \le 100\sigma$. Data extending over the full range of densities (such as shown in Fig. 1) are only taken up to a maximal size of $L=15.8\sigma$, while larger sizes up to $L=33.7\sigma$ have been studied only in the density range where the droplet (sph) exists. The sizes $L=50\sigma$ and $L=100\sigma$ have been used in the vicinity of the droplet evaporation/condensation transition (Sec. IV), where typical particle numbers N at the chosen temperature ($T=0.68T_c$) are near $N=15\,800$.

The first step of the simulation study addresses the estimation of the distribution function of the particle number $P_{\mu VT}(N)$ in the grand-canonical ensemble (at given chemical potential μ, volume $V=L^3$ and temperature T of the system). This distribution can be related to a Helmholtz free-energy function $F(N)$ via

$$F(N,V,T) = -k_B T \ln P_{\mu VT}(N) + \mu N + F_0, \tag{7}$$

where the constant F_0 is not important for our purposes. If $F(N,V,T)$ is given, we can define a chemical potential function as the derivative

$$\mu(N) \equiv \left(\frac{\partial F(N,V,T)}{\partial N}\right)_{VT} = -k_B T\left(\frac{\partial \ln P_{\mu VT}(N)}{\partial N}\right)_{VT} + \mu.$$

In the grand-canonical ensemble we observe an average value $\langle N\rangle_{\mu VT}$ such that $\mu(\langle N\rangle_{\mu VT})=\mu$, of course. However, in our study we are not only interested in the estimation of such average values but rather in the sampling of the full distribution $P_{\mu VT}(N)$ and thus the Landau free-energy function $F(N,V,T)$. This is done by successive umbrella sampling [66]. The range from $0<N<N_{max}$ is divided into a set of n_{max} windows of width λ,

$$[0,\lambda],[\lambda,2\lambda],\ldots[k\lambda,(k+1)\lambda],\ldots[(n_{max}-1)\lambda,n_{max}\lambda],$$

where $n_{max}\lambda=N_{max}$, and adjacent windows have the particle number at their boundary in common. In order to sample the histogram $H_k(N)$ corresponding to the kth window, the grand canonical moves where particles are inserted or deleted are constrained so that N falls in the considered window. The number n_{max} has to be chosen large enough so that $H_k(N)$ does not vary too much from the left boundary to the right boundary of the window [66,67]. Defining then $R_k=H_k[N=(k+1)\lambda]/H_k(N=k\lambda)$, the desired probability distribution is constructed successively and recursively,

$$P_{\mu VT}(N) = P_{\mu VT}(0)\prod_{i=0}^{k-1} R_i \frac{H_k(N)}{H_k(k\lambda)}, \tag{8}$$

where k in Eq. (8) is now the largest integer of the ratio N/λ.

For the study of the droplet evaporation/condensation transition, it turned out to be useful to work with a variant of this method, where one works in the canonical (NVT) ensemble but wishes to construct the distribution $P_{NVT}(U)$ of the total potential energy U in the system. The procedure was exactly as described above: the main distinction, however, is that the starting value of the iteration is a minimum energy U_0, while for the sampling of $P_{\mu VT}(N)$ the natural starting value is $N=0$, vanishing vapor density. In addition, U unlike N is a continuous variable, and so each window is arbitrarily divided into a suitable number of subintervals to obtain a convenient sampling of the corresponding histogram [67].

In order to locate the coexistence value $\mu=\mu_{coex}$ where vapor-liquid coexistence occurs in the bulk we need to work in the region of μ where $P_{\mu VT}(N)$ has two peaks, one peak near $N=V\rho_v$ and the other peak near $N=V\rho_\ell$. The phase transition occurs when the area underneath both peaks is equal [68,69]. For implementing this equal weight rule, standard histogram reweighting methods [70] were used,

$$P_{\mu' VT}(N) = \exp[(\mu'-\mu)N/k_B T]P_{\mu VT}(N). \tag{9}$$

In agreement with a previous estimation [63], phase coexistence at $T=0.68T_c$ was found for

$$\mu_{coex}(T)/k_B T = -4.755\,25. \tag{10}$$

Figure 3 shows the resulting Landau free-energy density $f_L(\rho,T)\equiv L^{-3}F(N,V,T)/k_B T$ plotted vs ρ at phase coexistence for six choices of L. The minima of this function yield the coexisting vapor ($\rho_v=0.009\,92\sigma^{-3}$) and liquid ($\rho_\ell=0.769\,17\sigma^{-3}$) densities. Near the minima polynomial fit functions are shown. Note that the undetermined constant F_0 in Eq. (7) was chosen such that $F(N,V,T)=0$ for $\rho=\rho_v$ for all L. Near the (parabolic) minima of these functions finite-size effects are completely negligible for the chosen temperature and range of L that was explored. The size dependence of $f_L(\rho,T)$ is entirely due to interfacial effects related to the different types of phase coexistence shown already in Fig. 1. Indeed, for $L\to\infty$ all these interfacial effects are negligibly small, and do not contribute to the bulk term of the free energy $f_L(\rho,T)$, which (in our normalization) can be written as

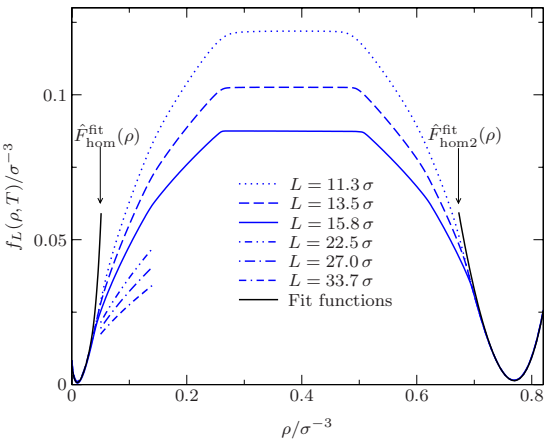

FIG. 3. (Color online) Normalized free-energy density $f_L(\rho,T) \equiv L^{-3}F(N,V,T)/k_BT$ plotted vs density ρ for six choices of L at $T=0.68T_c$. Only for the three smallest sizes the functions are shown over the full density range. The free-energy branches describing homogeneous vapor and liquid are fitted to simple polynomials of the density.

$$f_b(\rho,T) = \lim_{L\to\infty} f_L(\rho,T) = 0, \quad \rho_v \le \rho \le \rho_\ell. \tag{11}$$

The finite-size behavior of $f_L(\rho,T)$ observed in Fig. 3 contains important information on the interfacial free-energy contributions due to the various interfacial configurations that occur here (Fig. 1). This is precisely the basic idea of the present work: to accurately extract the information about the interfacial free energy of droplets (such as the droplet shown in Fig. 2) from data as shown in Figs. 1 and 3.

Already for a long time [61] it has been accepted that the slablike configuration in the region of the density ρ around the "diameter density" $\rho_d=(\rho_\ell+\rho_v)/2$ can be used to extract information on the vapor-liquid interfacial free energy of flat planar interfaces,

$$\gamma_{v\ell} = \lim_{L\to\infty} \frac{L}{2} f_L(\rho,T). \tag{12}$$

Of course, the factor $\frac{1}{2}$ in Eq. (12) results from the fact that we have two interfaces (of area $L\times L$) and not just a single interface. $f_L(\rho,T)$ in the region from ρ_{t3} to ρ_{t4} is strictly constant (apart from the immediate vicinity of the interfacial shape transitions at ρ_{t3} and ρ_{t4} to a cylindrical liquid or vapor domain, respectively). This indicates that a contribution due to interactions between both interfaces (which in our model will occur because of capillary wave-type fluctuations of the interfaces, for instance [17]) is also negligibly small already for the range of linear dimensions L that have been studied. Using Eq. (12) with our data, we find

$$\gamma_{v\ell} \approx 0.465 k_B T \sigma^{-2}, \tag{13}$$

an estimate which agrees accurately with previous studies [63]. Of course, for a test of the classical theory of homogeneous nucleation [Eqs. (1) and (2)] it is essential to know $\gamma_{v\ell}$ very accurately for precisely the same model for which the droplets are studied.

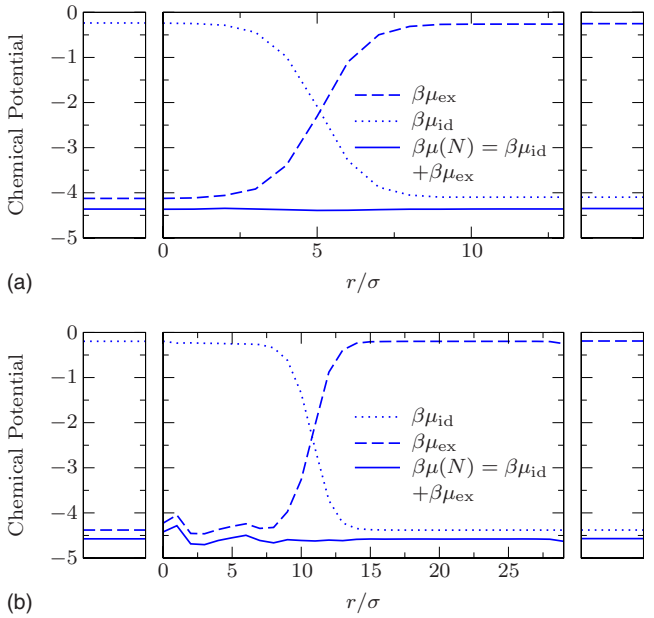

FIG. 4. (Color online) Radial distribution of the excess chemical potential $\mu_{ex}(r)$ (broken curves), the ideal gas part $\mu_{id}(r)$ (dotted curves) and their sum (full curves) for boxes of linear dimension $L=15.8\sigma$ (upper part) and $L=33.7\sigma$ (lower part) at density $\rho=0.1\sigma^{-3}$ and $T=0.68T_c$ (central part of the figure). The small pictures on the right and left sides show corresponding results for μ_{ex}, μ_{id} and $\mu(N)$ in bulk vapor and liquid phases at the densities ρ'_v,ρ'_ℓ as defined in Fig. 1. Note the different abscissa scales for r in the upper and lower part, respectively.

Finally we mention that we also have implemented the Widom test particle method [71] to measure the exchange chemical potential μ_{ex} which is related to the total chemical potential $\mu(N)$ via

$$\mu(N) = \mu_{id} + \mu_{ex}, \tag{14}$$

where μ_{id} is the known chemical potential of an ideal gas of N particles in the volume V. We have generalized this standard method, carrying out runs in the canonical (NVT) ensemble at densities $\rho=N/V$ in the range in between ρ_t and ρ_{t2}, to "measure" the radial profile $\mu_{ex}(r)$ together with the density profile $\rho(r)$ of droplets coexisting with vapor in the box. In each configuration that is analyzed the droplet is identified using the Stillinger connectivity criterion [40]; i.e., two particles are considered to be connected if their distance does not exceed 1.5σ. In this way the distribution function $P_{NVT}(N_c)$ of cluster sizes (i.e., N_c is the number of particles contained in a cluster) can be determined [54]. In the considered density region, the distribution has a peak at very small cluster sizes ($N_c<10$). In addition each configuration contains one very large cluster, which contains most of the particles in the system. We determine in each configuration which is analyzed the center of mass of the largest cluster and use this as the coordinate origin to record the density profile $\rho(r)$ and the profile $\mu_{ex}(r)$. Figure 4 shows the resulting profiles of $\mu_{ex}(r)$ and $\mu_{id}(r)$, together with corresponding "measurements" in bulk vapor and liquid phases, at the corresponding densities ρ'_v,ρ'_ℓ (Fig. 1). These results are an "ex-

perimental" proof that indeed very good chemical equilibrium between the liquid droplet and surrounding vapor is established, as it should be. While in our simulation the temperature is homogeneous, the homogeneity of the chemical potential is a less trivial requirement for full thermal equilibrium. There does not exist an excess contribution of the chemical potential due to the interface (and there should not be one [72] as the droplet can freely exchange particles with the surrounding vapor). The fact that droplet and surrounding vapor in the box can be treated as subsystems which are in full equilibrium with each other is the central starting point for the considerations on which our analysis of the droplet interfacial free energy is based, as is described in more detail in the following section.

III. DROPLET-VAPOR COEXISTENCE IN FINITE VOLUMES

A. General arguments

Here we follow the standard statements of the phenomenological theory of vapor-liquid equilibria [17,72] that one may choose conventions such that (in a one-component system) there is neither an excess of volume V nor an excess of particle number N to be attributed to the interface. Thus, for densities ρ that fall in the regime $\rho_t < \rho < \rho_{t2}$, we can divide up the volume and the particle numbers as follows:

$$V = V_\ell + V_v, \quad N = N_\ell + N_v, \tag{15}$$

where we also can take $V_\ell = 4\pi R^3/3$ to define the droplet radius R, since the average shape of the liquid droplet must be spherical. Note that we must choose ρ not to be to close to either ρ_t or ρ_{t2}, to strictly avoid fluctuations of the two-phase equilibrium to either the homogeneous vapor or cylinderlike droplets, respectively. This condition restricts the use of Eq. (15) and the analysis based on it to box linear dimensions L that must be much larger than σ. (Had we worked close to the vapor-liquid critical temperature T_c, the stronger condition $L \gg \xi$ would be required, where ξ is the correlation length of density fluctuations in the bulk). Of course, the box must always be sufficiently large so that there is enough space for the liquid droplet and surrounding vapor so that the phases are clearly distinguishable. This implicit condition also constrains the applicability of Eq. (15).

Now we simply state the vapor which we consider in Eq. (15) has a chemical potential difference $\hat{\mu}$ corresponding to the density ρ_v' (inset of Fig. 1) and the liquid has the density ρ_ℓ'. (These statements have been tested via direct observations, cf. Fig. 4, since μ_{id} is simply related to these densities.) Thus

$$N_\ell = \rho_\ell' V_\ell, \quad N_v = \rho_v' V_v, \tag{16}$$

and since $N = \rho V$ we can simply find V_ℓ from the observation (as shown in Fig. 1) which values of ρ_v', ρ_ℓ' belong to a chosen pair of values, V, N at given ρ:

$$V_\ell = V \frac{\rho - \rho_v'}{\rho_\ell' - \rho_v'}. \tag{17}$$

This is nothing but the lever rule of phase coexistence, which holds in finite geometry, too, due to the convention that there are no interface corrections either to the volume nor the particle number.

An important check of this argument is possible by noting that the same values of $\hat{\mu}, \rho_v', \rho_\ell'$ can be obtained by different choices of N and V, chosen such that the same droplet volume V_ℓ results. The argument that a system in full thermal equilibrium can be divided into subsystems, which may exchange particles and have the same chemical potential (difference) $\hat{\mu}$ [72] immediately shows that a large box containing vapor at density ρ_v' and a (relatively) small droplet of volume V_ℓ and density ρ_ℓ' can be (as a thought experiment), decomposed in a smaller box (still containing the droplet and surrounding vapor of density ρ_v') and the remaining volume containing only vapor of density ρ_v'. If different choices of N and V with the same $\hat{\mu}$ do not yield the same V_ℓ, it would be an indication that either part of the data are affected by the droplet evaporation/condensation transition, or the transition from the spherical to cylindrical droplet, or both: our analysis strictly implies that all microstates that are sampled under the given conditions do have the same droplet-vapor two-phase coexistence that was implied in Eqs. (15)–(17).

The final step in the argument is simply a related decomposition of the free-energy density $f_L(\rho, T)$,

$$f_L(\rho, T) = \frac{V_\ell}{V} f_L(\rho_\ell', T) + \frac{V_v}{V} f_L(\rho_v', T) + \frac{4\pi R^2}{V} \gamma(R). \tag{18}$$

Again the same argument of the additivity of subsystems coexisting with each other at the same chemical potential (difference) $\hat{\mu}$ imply that the free-energy density of the vapor is that of a bulk homogeneous vapor at density ρ_v' (which can be read off from data such as shown in Fig. 3). The liquid density is given by the bulk ρ_ℓ'. However, unlike V and N the free energy does contain an interfacial contribution, and in Eq. (18) we have specialized to the case of phase coexistence with a spherical droplet, allowing for an unknown surface free energy per unit area which we have denoted as $\gamma(R)$. Equation (18) does not make any assumption on $\gamma(R)$ and is simply the analog of Eq. (12) for flat interfaces where $\gamma_{v\ell}$ is extracted from the slab concentration. In the latter case $\hat{\mu} = 0$, however (cf. Figs. 1 and 3) and hence the analogs of the bulk vapor and liquid free-energy contributions, that are present in Eq. (18), do not occur in this case.

B. Phenomenological treatment of the droplet evaporation/condensation transition

The method to obtain $\gamma(R)$ that we have described above is limited to large R because of the transition to the cylinderlike geometry of the liquid droplet (Fig. 1). However, if we increase the linear dimension L of the box suitably, arbitrarily large values of R are accessible, at least in principle. (Of course, the demands for computer resources to equilibrate large droplets increase strongly with the droplet size.) Thus this limitation due to the transition of the droplet shape from spherical to cylindrical does not restrict the usefulness of the present methods in a serious way.

The situation is more subtle with respect to the droplet evaporation/condensation transition which prevents the applicability of our method for small R. Small values of R

correspond to small density differences $\rho-\rho_v$ in Fig. 1 [see Eq. (17)]. But the chosen density ρ must exceed ρ_t clearly, otherwise Eqs. (15)–(18) are not applicable. Since according to Eq. (17) at fixed R the density difference $\rho-\rho_v'$ scales like $1/L^3$, it must ultimately fall below $\rho_t-\rho_v$ [cf. Eq. (5)]; i.e., if we increase L at fixed R the equilibrium considered in the previous subsection always becomes unstable [50]. On the other hand, we must have a condition $L \gg \xi$, the correlation length of density fluctuations in the pure phases (near the critical point, the correlation length in the vapor and in the liquid are the same, while far below the critical point, they differ: however, in the context of these qualitative arguments this problem can be ignored). If this condition is not met, there would occur a non-negligible interaction between the droplet and its "images" in the image boxes created by the periodic boundary conditions, mediated via the tails of the liquid-vapor density profiles (remember that the "intrinsic" interfacial width of the interface, disregarding any capillary wave broadening, is 2ξ [17]).

For small droplets, where R does not exceed ξ much, our treatment loses its accuracy. One can no longer eliminate finite-size effects, as it can be expected, of course: for very small critical droplet size, any quasistatic description of nucleation loses its meaning. Rather than by rare (and hence well-separated) nucleation events many droplets, interacting with each other, form quickly, and the kinetics of phase separation of such a strongly supersaturated vapor rather resembles nonlinear spinodal decomposition [10,16], and Eq. (3) is no longer useful.

Thus it is important to characterize the droplet-evaporation transition more quantitatively, to clarify the extent to which this phenomenon is a practical limitation of our study of nucleation barriers. Here we briefly describe the general theoretical framework for this transition, following [53] where this transition was discussed for Ising ferromagnets.

Being interested in the asymptotic behavior for large L, where Eq. (5) is expected to hold [50], it is clear that ρ_v', ρ_ℓ' in Fig. 1 (inset) can deviate from ρ_v, ρ_ℓ only very little, and hence one can use linear expansions at the coexistence curve,

$$\rho_v' - \rho_v = \rho_v^2 k_B T \kappa_T^{(v)} \hat{\mu}, \quad \rho_\ell' - \rho_\ell = \rho_\ell^2 k_B T \kappa_T^{(\ell)} \hat{\mu}, \tag{19}$$

where $\kappa_T^{(\ell)}$ and $\kappa_T^{(v)}$ are the isothermal compressibilities at the vapor and liquid branches of the coexistence curve, respectively. This linear expansion of the densities corresponds to a quadratic expansion of the free energies of the pure vapor and liquid phases in Fig. 3, of course,

$$f_L^v(\rho,T) = \frac{1}{2}\rho_v^2 (k_B T)^2 \hat{\mu}^2 \kappa_T^{(v)},$$

$$f_L^\ell(\rho,T) = \frac{1}{2}\rho_\ell^2 (k_B T)^2 \hat{\mu}^2 \kappa_T^{(\ell)}. \tag{20}$$

For large L the radius R is also large and we may make the capillarity approximation, i.e., the R dependence of $\gamma(R)$ in Eq. (18) is neglected. With these assumptions, the thermodynamic potential in Eq. (18) is explicitly known, using also the relation between R and μ that holds in this limit in equilibrium [cf. Eq. (1)] and using the relation $\rho=(\partial p/\partial\mu)_{VT}$ to expand Δp linearly in $\hat{\mu}$, $\Delta p = k_B T \hat{\mu}(\rho_\ell - \rho_v)$. Hence

$$R = \frac{2\gamma_{v\ell}}{k_B T \hat{\mu}(\rho_\ell - \rho_v)}. \tag{21}$$

At the droplet evaporation/condensation transition the free-energy branch of the inhomogeneous system (droplet plus surrounding supersaturated vapor) intersects the free energy of the homogeneous (but more strongly) supersaturated gas, which according to Eqs. (19) and (20) is

$$f_\ell^v(\rho,T) = \frac{1}{2}\frac{(\rho-\rho_v)^2}{\rho_v^2}\frac{1}{\kappa_T}. \tag{22}$$

Equation (17) provides a relation between ρ and ρ_v' and, using Eq. (21), R can be eliminated in favor of $\hat{\mu}$. Note, however, that at the droplet evaporation/condensation transition the chemical potential difference of the homogeneous phase $\hat{\mu}_t'$ without the droplet, due to the larger supersaturation, is larger than the chemical potential $\hat{\mu}_t$ of the inhomogeneous phase at the transition point (Fig. 5).

With some algebra [53,54,56,67] one can obtain explicit expressions for both $\hat{\mu}_t$ and $\hat{\mu}_t'$ as well as ρ_t from the above relations, and thus justify Eq. (5). Of course, this treatment neglects the finite-size rounding of the transition, and since both $\hat{\mu}_t$ and $\hat{\mu}_t'$ vanish as $L\to\infty$,

$$\hat{\mu}_t' = 2\hat{\mu}_t \propto L^{-3/4}, \tag{23}$$

as well as $\rho_t-\rho_v$ [Eq. (5)]. It is a subtle issue to which extent a "sharp" transition can be observed. However, phenomenological arguments [53] indicate that the width $\Delta\rho$ over which the transition is rounded decreases with a larger power of $1/L$ than $(1/L)^{3/4}$, and hence in the limit of $L\to\infty$ the transition becomes asymptotically sharp. This is consistent with the previous [54,56] observations of this transition, although quantitative aspects [such as the $\frac{3}{4}$ exponent in the power laws, Eqs. (5) and (23)] could only roughly be confirmed (apart from work on the two-dimensional Ising model [58], where the predicted exponent is $\frac{2}{3}$ [52,53]). We shall address this issue in the next section.

IV. MONTE CARLO RESULTS ON THE DROPLET EVAPORATION/CONDENSATION TRANSITION

In previous work on the same model [54], it was already observed that the peak of the $\hat{\mu}$ vs ρ curve (Fig. 1) that is strongly rounded and almost symmetric around the position of the maximum for small L becomes rather sharp and asymmetric. Hence it resembles more and more the theoretical cusp shape (Fig. 5), as L increases, but a clear confirmation of the theory was not achieved.

Therefore we have reconsidered this problem in the present work, using successive umbrella sampling with respect to the energy distribution (see Sec. II) in the region near ρ_t. Already in Ref. [54] it was found that the transition can be observed by looking at the bimodal distribution function for various quantities (chemical potential $\hat{\mu}$, particle number of the largest cluster N_c, internal energy). It was found that the distribution of the internal energy suffers

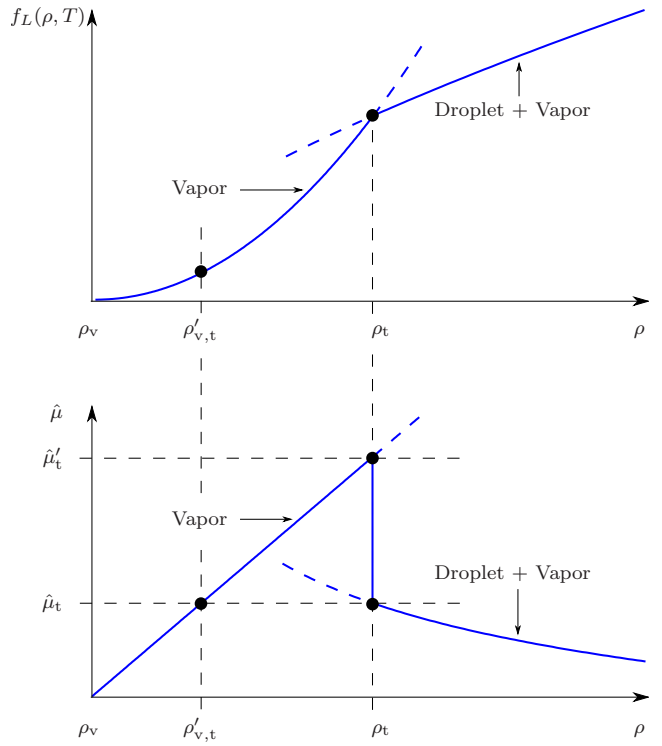

FIG. 5. (Color online) Graphical illustration of the equations used to locate the droplet evaporation/condensation transition by an approximate analytical calculation. At the transition density ρ_t, the free energy of the state containing a droplet plus surrounding vapor (Fig. 1) and of the state with the denser vapor without a droplet are equal (upper part). The density $\rho'_{v,t}$ of the vapor surrounding the droplet at the transition point can be found from the equality of the chemical potentials ($\hat{\mu}_t$), lower part. Using Eq. (21), $\hat{\mu}_t$ yields the corresponding value of R, and Eq. (17) then yields the relation between ρ_t and L. Both in the plot of $f_L(\rho,T)$ vs ρ (upper part) and in the plot of $\hat{\mu}$ vs ρ (lower part) metastable parts of the branches are shown as broken curves, and the finite size rounding seen in Figs. 1 and 3 due to the fact that in a finite simulation box the system can jump back and forth between both states is disregarded.

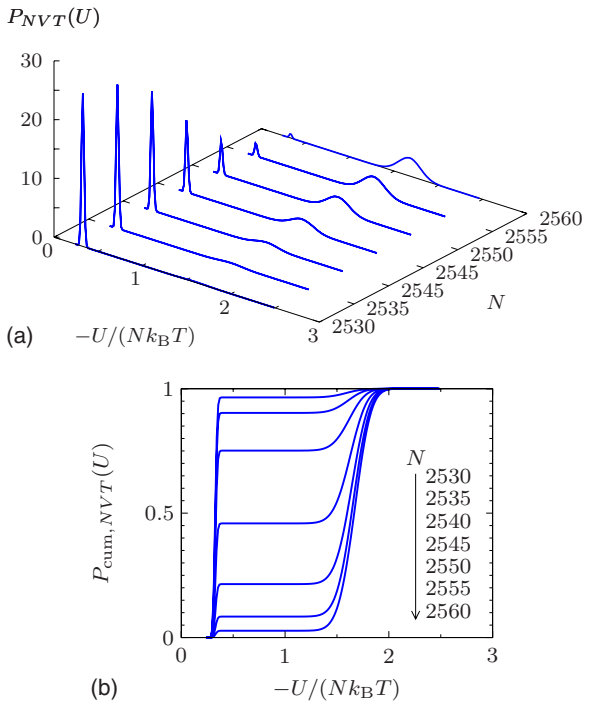

FIG. 6. (Color online) Probability distributions $P_{NVT}(U)$ plotted versus energy per particle $-U/(Nk_BT)$ for seven values of N, for $T=0.68T_c$, and a cubic box with linear dimension $L=50\sigma$ (upper part). Cumulative distribution function $P_{cum,NVT}(U)$ for the same cases (lower part).

much less from statistical errors than the other quantities and it is also easy to measure. Therefore we use the internal energy distribution $P_{NVT}(U)$ throughout this work (for more details see [67]). Figure 6 gives a typical example for the variation in $P_{NVT}(U)$ with N. We impose the standard "equal area rule" [68,69] for the location of this first-order transition: the transition density ρ_t (or equivalently, the corresponding particle number $N_t=\rho_t L^3$) occurs when both peaks in Fig. 6 have equal weight. Note that the widths of the peaks are strikingly different—fluctuations are relatively small for the "pure" vapor and relatively large for the system exhibiting the coexistence between liquid droplet and surrounding vapor. Therefore it is useful to consider the integral of the distribution

$$P_{cum,NVT}(U) = \int_0^U dU' P_{NVT}(U'), \tag{24}$$

since this function shows a plateau, when $x=-U/k_BTN$ exceeds the normalized energy in the vapor and rises to a second plateau $P_{cum,NVT}(U)=1$ when x exceeds the normalized energy of the droplet coexisting with the vapor, due to the normalization of probability. Thus, when we find a well-developed first plateau, it displays the relative weight w_{NVT} of the pure vapor state and the condition $w_{NVT}=\frac{1}{2}$ yields N_t. While for small L such as $L=22.5\sigma$ the two distributions overlap in their wings, and hence only an inflection point is found [67] rather than a well-defined plateau, for large L such as $L=50\sigma$ the two peaks of $P_{NVT}(U)$ are very well separated from each other, and the plateau is clearly defined (Fig. 6). Thus, $N_t=2544\pm1$ can be estimated with very good accuracy.

When one examines these data for $\rho_t-\rho_v$ on a log-log plot versus L, disappointingly there occurs a pronounced curvature (Fig. 7). Obviously, there are still corrections to the asymptotic behavior [Eqs. (5) and (23)] present, so that a simple power law (without any higher order terms) does not yet suffice. Of course, comparing the actual data for $\hat{\mu}$ vs ρ (Fig. 1) with the idealized hypothetical description (Fig. 5), it is clear that ρ_t does not occur close enough to ρ_v that the simple linearization approximation [which is used in Eq. (19) and underlies Eq. (22) as well] is accurate. To study the extrapolation to the thermodynamic limit, we have fitted straight lines through three successive data points in Fig. 7, to obtain "effective exponents," as quoted in the figure. A plot of these effective exponents vs $1/L$ clearly suggests that the asymptotic value for $L\to\infty$ is indeed $\frac{3}{4}$, as expected (Fig. 7).

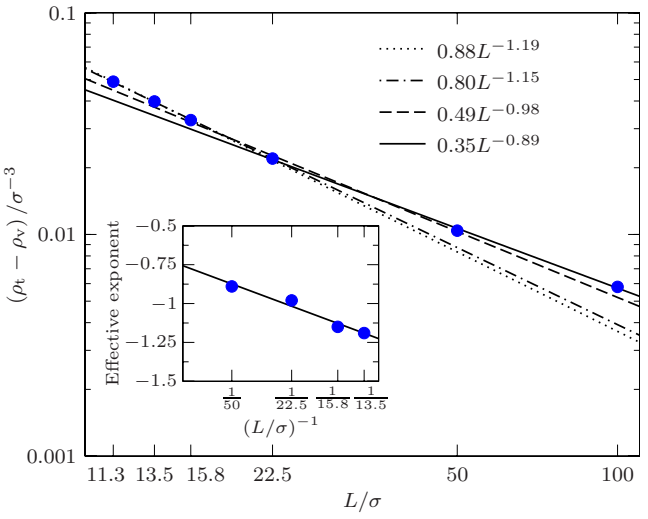

FIG. 7. (Color online) Log-log plot of the density difference $\rho_t - \rho_v$ versus the system size L for $T/T_c = 0.68$. Straight lines exhibit power-law fits through three successive values (slopes being indicated in the figure). Inset: plot of the "effective exponent," as estimated before versus the inverse system size L^{-1}.

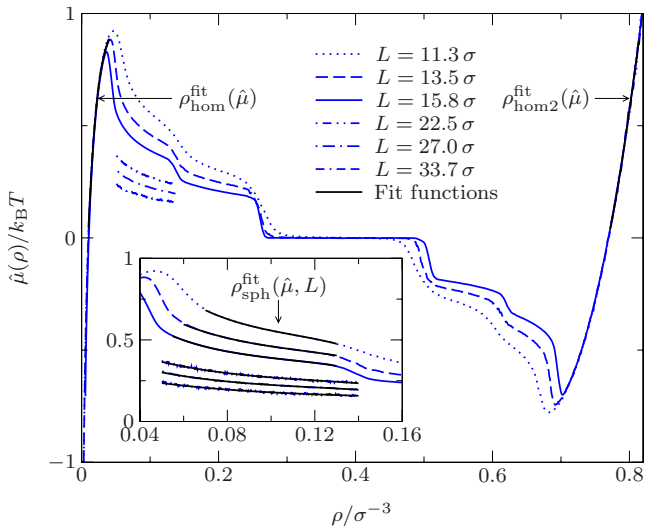

FIG. 8. (Color online) Chemical potential difference $\hat{\mu}(\rho)$ plotted vs the density ρ at $T = 0.68T_c$ including data for six choices of L. The part of the curves describing pure homogeneous vapor and pure homogeneous liquid that are not affected by finite-size effects due to two-phase coexistence are fitted by functions $\rho^{\text{fit}}_{\text{hom}}(\hat{\mu}) = -0.823 + 110.04\hat{\mu} - 2518.1\hat{\mu}^2 + 20\,910\hat{\mu}^3$ and $\rho^{\text{fit}}_{\text{hom2}}(\hat{\mu}) = 702.08 - 2628.4\hat{\mu} + 3255.8\hat{\mu}^2 - 1333\hat{\mu}^3$, respectively. The inset shows a magnified plot of the $\hat{\mu}(\rho)$ vs ρ curves in the region of interest, where two-phase coexistence between a droplet and surrounding vapor always occurs. In this region the data were also fitted by polynomials $\rho^{\text{fit}}_{\text{sph}}(\hat{\mu}, L)$, which now distinctly depend on L.

V. MONTE CARLO RESULTS FOR THE SURFACE FREE ENERGY OF LIQUID DROPLETS

In this section we now apply the description presented in Eq. (18) to obtain the surface free energy of droplets as function of the droplet radius R. For this purpose, data for $f_L(\rho, T)$ such as shown in Fig. 3 are used, and we use the $\hat{\mu}$ vs ρ data (cf. Fig. 1), as explained in Sec. III, to infer the volume of the (spherical) liquid droplet using Eq. (17). In this case the identification of the liquid droplet in terms of the Stillinger [40] neighborhood criterion is not required. While the latter method is almost fully compatible with the present method at the (low) temperature $T = 0.68T_c$ as has been discussed in Sec. II, we feel that the latter method will become problematic at temperatures closer to T_c, where the difference between ρ_ℓ and ρ_v becomes much smaller and ultimately vanishes. The method to identify the liquid droplet from "measurements" of the functions $\hat{\mu}(\rho)$ and $f_L(\rho, T)$ should not suffer from this problem, of course, and should work, in principle, arbitrarily close to T_c (if simulations for large enough L are feasible).

Figure 8 presents our data for $\hat{\mu}(\rho)$ vs ρ for six different choices of L. The full variation $(0 < \rho < 0.81)$ has been recorded for the three smallest sizes, however, while for the three larger sizes only the region where the droplet coexists with surrounding vapor is included. Figure 8 demonstrates that for the relevant regimes of densities both the density of the pure gas and the density of the pure liquid do not depend on L, within the accuracy of our simulation. Thus, $\rho'_v(\hat{\mu})$ and $\rho'_\ell(\hat{\mu})$, needed in Eq. (17), can be determined uniquely. For this purpose, it was convenient to use polynominal fit functions $\rho^{\text{fit}}_{\text{hom}}(\hat{\mu})$ and $\rho^{\text{fit}}_{\text{hom2}}(\hat{\mu})$, as shown in Fig. 8. The variation in $\hat{\mu}(\rho)$ vs ρ in the region of interest, where coexistence between the liquid drop with surrounding vapor occurs, was also described by analytic fit functions to facilitate the use of Eqs. (17) and (18). As described in Sec. III, we can use the explicit knowledge of $f_L(\rho'_\ell, T)$ of the pure liquid and of $f_L(\rho'_v, T)$ of pure vapor, together with our knowledge of the total free energy $f_L(\rho, T)$ (Fig. 3) and the knowledge of the volume fractions V_ℓ/V, $V_v/V = 1 - V_\ell/V$, to obtain accurate estimates of $4\pi R^2\gamma(R)$. The important consistency check that we have applied extensively is the fact that different choices of L yield data in overlapping regions of R: indeed we find (for $L = 11.3\sigma$, 13.5σ, and 15.8σ) that these data coincide within our statistical errors, and hence finite-size effects are negligibly small. In order to include the data for $L = 22.5\sigma$, 27.0σ, and 33.7σ, for which we did not record the full curve of $f_L(\rho, T)$ in the vicinity of the condensation/evaporation transition, we know $f_L(\rho, T)$ from the numerical integration of the $\hat{\mu}(\rho)$ vs ρ curves for these linear dimensions only up to a constant. Estimating these constants from least-squares fits, the data again fall on top of the data for the smaller values of L. This allows us to extend the curve to much larger values of R. Figure 9 shows the final result. Since the results on this large scale are hardly distinguishable from the classical capillarity prediction, $4\pi R^2\gamma_{v\ell}$, two insets are shown where these functions are shown on greatly magnified scales. It can be seen that in the region where $54 \le 4\pi R^2\gamma_{v\ell} \le 150$ the capillarity approximation overestimates the actual surface free energy $4\pi R^2\gamma(R)$ slightly. Even on these magnified scales, no systematic differences between our different choices for L can be seen, demonstrating our assertion that the present study is not affected significantly by finite-size effects. However, there emerges a slight but systematic difference between results where the proposed methods based on "macroscopic" measurements (curves labeled by "m") and between

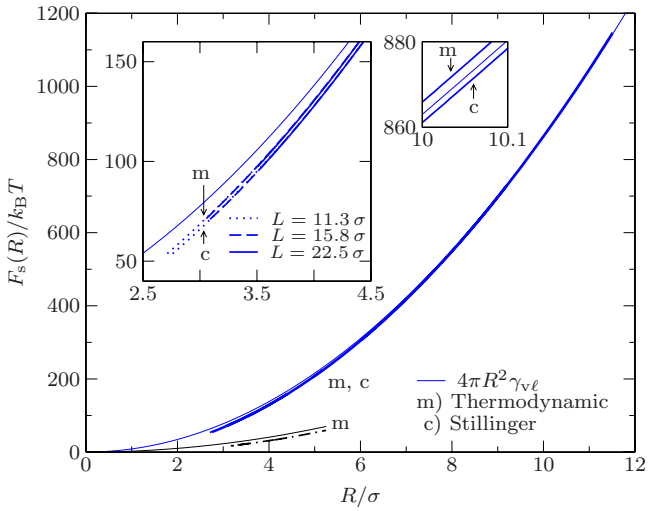

FIG. 9. (Color online) Surface free energy $F_s(R)=4\pi R^2\gamma(R)$ plotted vs the droplet radius R for $T=0.68T_c$. The thin full curve shows the result of the classical capillarity approximation $4\pi R^2\gamma_{v\ell}$, with $\gamma_{v\ell}$ taken from the independent estimation given in Eq. (13). The insets show magnified plots near $R=10\sigma$ (right) and from $R=2.5\sigma$ to $R=4.5\sigma$ (left). The curves labeled "m" are the results where R was computed from Eqs. (15)–(17), while the curves labeled "c" refer to estimations of R from the Stillinger [40] cluster criterion. For $T=0.85T_c$ analogous data are shown for small radii up to $R=5.25\sigma$ (only for method "m").

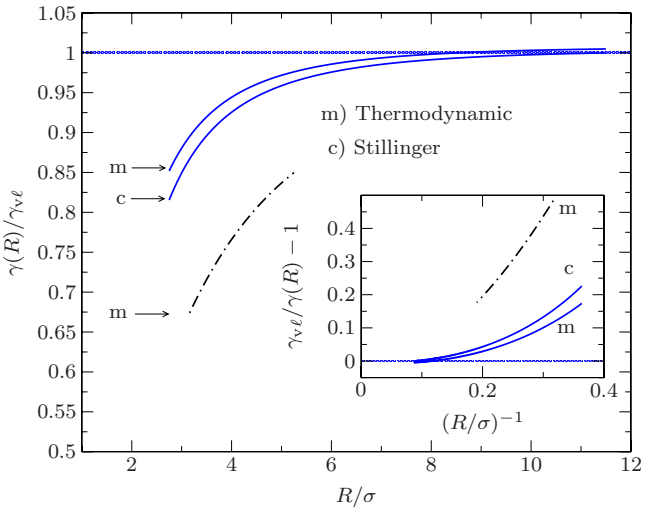

FIG. 10. (Color online) Plot of $\gamma(R)/\gamma_{v\ell}$ vs the droplet radius R for $T=0.68T_c$ (full curves) and for $T=0.85T_c$ (broken curve). The curve labeled by "m" has been obtained using "macroscopic measurements" of ρ_v', ρ_ℓ' and applying Eqs. (15)–(17) to estimate R, while the curve labeled by "c" has been obtained from observations of the droplets identified via the Stillinger connectivity criterion [40]. Inset: the plotted data vs the inverse radius reveals that the deviation from the classical capillarity approximation cannot be described by a Tolman correction, at least not for $T=0.68T_c$. Otherwise the curve would be a straight line through the origin with slope 2δ.

results based on the Stillinger cluster criterion (curves labeled by "c") are used. The latter always yield slightly smaller energies. In the region which is physically meaningful for nucleation experiments, shown in the left inset, this difference between the curves labeled by "m" and by "c" is much smaller than the deviation of both curves from the conventional classical nucleation theory. Remember that Eq. (2) can be written as $\Delta F^*=4\pi R^2\gamma_{v\ell}/3$, so the barrier is 1/3 of the surface energy, and hence the left inset of Fig. 9 corresponds to a region of $18\leq\Delta F^*/k_BT\leq 50$. The right inset shows that the difference between the predictions resulting from the two cluster definitions persists for large cluster sizes, but remains of the order of a few k_BT (and then the relative difference is below 1%). For the higher temperature $T=0.85T_c$ the surface free energy of the droplets is smaller. Figure 9 shows data up to a droplet radius of $R=5.25\sigma$ and the corresponding classical capillarity prediction. The deviation is slightly larger than for the lower temperature. Similar behavior has already been observed in [62].

With decreasing R the relative deviation between $4\pi R^2\gamma_{v\ell}$ and the actual $4\pi R^2\gamma(R)$ increases and reaches about 15% for $R\approx 3\sigma$ (Fig. 10). However, for ΔF^* this corresponds to a difference of a few k_BT. It is also interesting to observe that the relative deviation from unity decreases with increasing R much faster than one would expect from a Tolman correction, Eq. (4): it is impossible to extract a Tolman length δ from Eq. (7) in any meaningful way as shown in the inset of Fig. 10. These findings are very similar to the results of ten Wolde and Frenkel [41] for a closely related model using a Stillinger-type criterion to define liquid droplets. They concluded that the classical nucleation theory works for $T=0.68T_c$, apart from a small offset of the barrier, but a Tolman correction could not be identified either.

VI. CONCLUSIONS

In this paper, we have presented a method by which the surface free energy of liquid droplets coexisting with surrounding vapor can be obtained for a wide range of droplet radii. We have demonstrated the feasibility of this method using a simple fluid where particles interact with (truncated) Lennard-Jones forces as an example. This method generalizes the standard method, where the interfacial free energy of flat interfaces is extracted from the density probability distribution in a finite-sized box, to curved interfaces. This generalization is not completely straightforward because one must take into account that the vapor coexisting in a finite volume with a liquid droplet is supersaturated, in comparison with a vapor at bulk vapor-liquid density, and also the liquid droplet has an enhanced density. We have shown systematically that these effects can be considered, applying general concepts of statistical mechanics about phase equilibria, but one must avoid using simulation data affected by the evaporation/condensation transition of the droplet. We confirm the phenomenological prediction that the density ρ_t, at which this transition occurs, differs from the vapor density at coexistence ρ_v, via a power-law correction, $\rho_t-\rho_v\propto L^{-3/4}$, where L is the linear dimension of the simulation box.

Our method, based on "macroscopic measurements" to characterize the two-phase equilibrium in the finite box, is compared with the standard method based on the "micro-

scopic" identification of liquid droplets in terms of the Stillinger neighborhood criterion, and found to be at low temperatures in almost perfect agreement with the latter method. We argue, however, that our method is superior since it is applicable also close to the critical point, while the microscopic approach would be hampered by the percolation of liquid droplets in the vapor phase. (Such an effect is well known in the lattice gas models of fluids [73].) In addition, the generalization of our method to the case of cylindrical droplets or bubble nucleation in liquids as depicted in Fig. 1 should be completely straightforward.

We find that the surface free energy $\gamma(R)$ of the droplets moves toward the interface tension $\gamma_{v\ell}$ of flat interfaces rather fast with increasing R, Fig. 10, the results cannot be described by a Tolman-type correction. This result is in full accordance with a rather different simulation analysis for a related model presented earlier by ten Wolde and Frenkel [41]. The deviations between $4\pi R^2\gamma(R)$ and the classical prediction $4\pi R^2\gamma_{v\ell}$ are nowhere large. These deviations cannot explain the large deviations between the nucleation rates predicted from the classical theory of nucleation and the corresponding measurements in liquid argon at low temperatures [26]. If these measurements are correct, other explanations (rather than a very strong deviation of $\gamma(R)$ from $\gamma_{v\ell}$) must be sought [nucleation of fluid droplets at low vapor density is a kinetic process and it is not certain that the assumption that a critical droplet is formed, which is in some kind of equilibrium with surrounding vapor under isothermal conditions, as implied by Eqs. (2) and (3), holds]. As a consequence, it is desirable to generalize our approach to various other systems to elucidate better the conditions under which classical nucleation theory holds and clarify the dependence of the droplet interfacial tension $\gamma(R)$ on the droplet radius R. Extensions to heterogeneous nucleation are currently investigated by our group [74].

[1] M. Volmer and A. Weber, Z. Phys. Chem. **119**, 277 (1926).
[2] R. Becker and W. Döring, Ann. Phys. **416**, 719 (1935).
[3] Ya. B. Zeldovitch, Acta Physicochim. URSS **18**, 1 (1943).
[4] J. E. Burke and D. Turnbull, Prog. Met. Phys. **3**, 220 (1952).
[5] J. Frenkel, *Kinetic Theory of Liquids* (Dover, New York, 1955).
[6] J. Feder, K. C. Russell, J. Lothe, and G. M. Pound, Adv. Phys. **15**, 111 (1966).
[7] J. S. Langer, Ann. Phys. (N.Y.) **41**, 108 (1967); **54**, 258 (1969); **65**, 53 (1971).
[8] *Nucleation*, edited by A. C. Zettlemoyer (M. Dekker, New York, 1969).
[9] F. F. Abraham, *Homogeneous Nucleation Theory* (Academic, New York, 1974).
[10] K. Binder and D. Stauffer, Adv. Phys. **25**, 343 (1976).
[11] K. Binder, Rep. Prog. Phys. **50**, 783 (1987).
[12] H. Reiss, A. Tabazadeh, and J. Talbot, J. Chem. Phys. **92**, 1266 (1990).
[13] D. W. Oxtoby, J. Phys.: Condens. Matter **4**, 7627 (1992); A. Laaksonen, V. Talanquer, and D. W. Oxtoby, Annu. Rev. Phys. Chem. **46**, 489 (1995).
[14] D. Kashchiev, *Nucleation: Basic Theory with Applications* (Butterworth-Heinemann, Oxford, 2000).
[15] *Nucleation, Compt. Rendus Physique*, Vol. 7 (2006), special issue, edited by S. Balibar and J. Villain.
[16] K. Binder, in *Kinetics of Phase Transitions*, edited by S. Puri and V. Wadhawan (CRC Press, Boca Raton, 2009), Chap. 2.
[17] J. S. Rowlinson and B. Widom, *Molecular Theory of Capillarity* (Clarendon, Oxford, 1982).
[18] R. C. Tolman, J. Chem. Phys. **17**, 333 (1949).
[19] M. A. Anisimov, Phys. Rev. Lett. **98**, 035702 (2007).
[20] E. M. Blokhuis and D. Bedeaux, J. Chem. Phys. **97**, 3576 (1992).
[21] M. J. Haye and C. Bruin, J. Chem. Phys. **100**, 556 (1994).
[22] V. Talanquer and D. W. Oxtoby, J. Phys. Chem. **99**, 2865 (1995).
[23] M. E. Fisher, Physics **3**, 255 (1967).
[24] M. Müller, L. G. MacDowell, P. Virnau, and K. Binder, J. Chem. Phys. **117**, 5480 (2002).
[25] Y. Viisanen, R. Strey, and H. Reiss, J. Chem. Phys. **99**, 4680 (1993).
[26] A. Fladerer and R. Strey, J. Chem. Phys. **124**, 164710 (2006).
[27] K. Iland, J. Wölk, R. Strey, and D. Kashchiev, J. Chem. Phys. **127**, 154506 (2007).
[28] M. P. Allen and D. J. Tildesley, *Computer Simulation of Liquids* (Clarendon, Oxford, 1989).
[29] K. Binder and H. Müller-Krumbhaar, Phys. Rev. B **9**, 2328 (1974).
[30] D. Stauffer, A. Coniglio, and D. W. Heermann, Phys. Rev. Lett. **49**, 1299 (1982).
[31] D. Stauffer, Int. J. Mod. Phys. C **10**, 809 (1999).
[32] V. A. Shneidman, K. A. Jackson, and K. M. Beatty, J. Chem. Phys. **111**, 6932 (1999); Phys. Rev. B **59**, 3579 (1999).
[33] S. Wonczak, R. Strey, and D. Stauffer, J. Chem. Phys. **113**, 1976 (2000).
[34] P. G. Bolhuis, C. Dellago, D. Chandler, and P. Geissler, Annu. Rev. Phys. Chem. **53**, 291 (2002).
[35] A. C. Pan and D. Chandler, J. Phys. Chem. B **108**, 19681 (2004).
[36] L. Maibaum, Phys. Rev. Lett. **101**, 019601 (2008).
[37] J. K. Lee, J. A. Barker, and F. F. Abraham, J. Chem. Phys. **58**, 3166 (1973).
[38] A. Nußbaumer, E. Bittner, T. Neuhaus, and W. Janke, Europhys. Lett. **75**, 716 (2006).
[39] K. Binder, J. Chem. Phys. **63**, 2265 (1975).
[40] F. H. Stillinger, J. Chem. Phys. **38**, 1486 (1963).
[41] P. R. ten Wolde and D. Frenkel, J. Chem. Phys. **109**, 9901 (1998).
[42] P. R. ten Wolde, M. J. Ruiz-Montero, and D. Frenkel, J. Chem. Phys. **110**, 1591 (1999).
[43] G. M. Torrie and J. P. Valleau, J. Comput. Phys. **23**, 187 (1977).
[44] D. Frenkel and B. Smit, *Understanding Molecular Simulation: From Algorithms to Applications* (Academic, San Diego,

2002).
[45] S. Auer and D. Frenkel, Nature (London) **409**, 1020 (2001).
[46] S. Auer and D. Frenkel, Nature (London) **413**, 711 (2001).
[47] A. Cacciuto, S. Auer, and D. Frenkel, Nature (London) **428**, 404 (2004).
[48] T. Schilling and D. Frenkel, Phys. Rev. Lett. **92**, 085505 (2004).
[49] T. Schilling and D. Frenkel, Comput. Phys. Commun. **169**, 117 (2005).
[50] K. Binder and M. H. Kalos, J. Stat. Phys. **22**, 363 (1980).
[51] H. Furukawa and K. Binder, Phys. Rev. A **26**, 556 (1982).
[52] M. Biskup, L. Chayes, and R. Kotecky, Europhys. Lett. **60**, 21 (2002).
[53] K. Binder, Physica A **319**, 99 (2003).
[54] L. G. MacDowell, P. Virnau, M. Müller, and K. Binder, J. Chem. Phys. **120**, 5293 (2004).
[55] E. A. Carlen, M. C. Carvalho, R. Esposito, J. L. Lebowitz, and R. Marra, Mol. Phys. **103**, 3141 (2005).
[56] L. G. MacDowell, V. K. Shen, and J. R. Errington, J. Chem. Phys. **125**, 034705 (2006).
[57] R. Godawat, S. N. Jamadagni, J. R. Errington, and S. Garde, Ind. Eng. Chem. Res. **47**, 3582 (2008).
[58] A. Nußbaumer, E. Bittner, T. Neuhaus, and W. Janke, Europhys. Lett. **75**, 716 (2006).
[59] S. S. Martinos, A. Malakis, and I. Hadjiagapiou, Physica A **384**, 368 (2007).
[60] E. S. L. Oscar and E. V. Albano, Europhys. Lett. (to be published).
[61] K. Binder, Phys. Rev. A **25**, 1699 (1982).
[62] P. Virnau, M. Müller, L. G. MacDowell, and K. Binder, New J. Phys. **6**, 7 (2004).
[63] P. Virnau, M. Müller, L. G. MacDowell, and K. Binder, Comput. Phys. Commun. **147**, 378 (2002); J. Chem. Phys. **121**, 2169 (2004).
[64] J. Potoff and A. Panagiotopolous, J. Chem. Phys. **112**, 6411 (2000).
[65] B. M. Mognetti, L. Yelash, P. Virnau, W. Paul, K. Binder, M. Müller, and L. G. MacDowell, J. Chem. Phys. **128**, 104501 (2008).
[66] P. Virnau and M. Müller, J. Chem. Phys. **120**, 10925 (2004).
[67] More details can be found in M. Schrader, *Diplomarbeit*, Johannes-Gutenberg-Universität Mainz, 2009.
[68] K. Binder and D. P. Landau, Phys. Rev. B **30**, 1477 (1984).
[69] C. Borgs and R. Kotecky, J. Stat. Phys. **61**, 79 (1990).
[70] A. M. Ferrenberg and R. H. Swendsen, Phys. Rev. Lett. **61**, 2635 (1988).
[71] B. Widom, J. Chem. Phys. **39**, 2808 (1963).
[72] L. D. Landau and E. M. Lifshitz, *Statistical Physics* (Pergamon Press, Oxford, 1958).
[73] H. Müller-Krumbhaar, Phys. Lett. **48A**, 459 (1974); **50A**, 27 (1974).
[74] D. Winter, P. Virnau, and K. Binder, J. Phys.: Condens. Matter (to be published).